Karaelmas Science and Engineering Journal
Journal home page: https://dergipark.org.tr/tr/pub/karaelmasfen
DOI: 10.7212/karaelmasfen.1452945

Research Article
Received / Geliş tarihi : 14.03.2024
Accepted / Kabul tarihi : 09.08.2024

Characteristics and Kinetic Analysis of Sorption Performance of Functionalised Biomass by Various Acidic Agents

Çeşitli Asidik Ajanlar ile Fonksiyonelleştirilmiş Biyokütlenin Özellikleri ve Sorpsiyon Performansının Kinetik Analizi

Sahra Dandil*

Bilecik Şeyh Edebali University, Faculty of Engineering, Department of Chemical Engineering, Bilecik, Türkiye

Abstract

In this study, kiwi fruit peels were functionalized using hydrochloric acid (HCl), sulfuric acid (H_2SO_4) and phosphoric acid (H_3PO_4). The properties of the functionalized materials were determined. Fourier transform infrared spectrometer (FTIR) used to show functional groups caused by the agents. Crystalline or amorphous structure clarified by X-ray diffraction (XRD) analysis. Scanning electron microscope (SEM) revealed the changes by acidic agents on the surface of kiwi peel. The elemental composition was examined using energy-dispersive X-ray spectroscopy (EDX) analysis. The performance of kiwi peels functionalized with different acidic agents in sorption experiments were investigated. Kiwi peel functionalized with hydrochloric acid (HAFKP), kiwi peel functionalized with sulphuric acid (SAFKP), and kiwi peel functionalized with phosphoric acid (PAFKP) exhibited 94.53, 98.62, and 96.76% sorption, respectively, from 50 mL of 10 mg/L dye solution for 0.1 g after 24 h. The data obtained for the sorption of the materials were evaluated with kinetic models. Pseudo-first order, pseudo-second order, Elovich and Bangham models considered the processes as time-dependent. The processes carried out with HAFKP and PAFKP were fit the pseudo-second order kinetic model and determined to interact strongly with dye via chemical bonds. SAFKP, on the other hand, interacts physically with dye according to the pseudo-first order kinetic model.

Keywords: Characterization, functionalization, kinetics, kiwi.

Öz

Bu çalışmada kivi kabukları hidroklorik asit (HCl), sülfürik asit (H_2SO_4) ve fosforik asit (H_3PO_4) kullanılarak fonksiyonelleştirildi. Fonksiyonelleştirilmiş malzemelerin özellikleri belirlendi. Ajanların neden olduğu fonksiyonel grupları göstermek için Fourier dönüşümlü kızılötesi spektrometresi (FTIR) kullanıldı. X-ışını kırınımı (XRD) analiziyle kristal veya amorf yapı açıklandı. Taramalı elektron mikroskobu (SEM), kivi kabuğunun yüzeyinde asidik ajanların neden olduğu değişiklikleri ortaya koydu. Elementel bileşim, enerji dağılımlı X-ışını spektroskopisi (EDX) analizi kullanılarak incelendi. Farklı asidik ajanlarla fonksiyonelleştirilen kivi kabuklarının sorpsiyon deneylerindeki performansı araştırıldı. Hidroklorik asit ile fonksiyonelleştirilmiş kivi kabuğu (HAFKP), sülfürik asit ile fonksiyonelleştirilmiş kivi kabuğu (SAFKP) ve fosforik asit ile fonksiyonelleştirilmiş kivi kabuğu (PAFKP) 0.1 g için 24 saat sonra 50 mL'lik 10 mg/L boya çözeltisinden sırasıyla % 94.53, 98.62 ve 96.76 sorpsiyon sergiledi. Malzemelerin sorpsiyonu için elde edilen veriler kinetik modellerle değerlendirildi. Yalancı birinci derece, yalancı ikinci derece, Elovich ve Bangham modelleri prosesleri zamana bağlı olarak ele aldı. HAFKP ve PAFKP ile gerçekleştirilen proseslerin yalancı ikinci derece kinetik modele uyduğu ve boya ile kimyasal bağlar yoluyla kuvvetli etkileşime girdikleri belirlendi. SAFKP ise yalancı birinci dereceden kinetik modele göre boya ile fiziksel olarak etkileşime girdi.

Anahtar Kelimeler: Karakterizasyon, fonksiyonelleştirme, kinetikler, kivi.

*Corresponding author: sahra.ugur@bilecik.edu.tr

Sahra Dandil orcid.org/0000-0001-9724-5597

1. Introduction

Biomass is agricultural and industrial materials such as wood, annual crops, and agricultural and forestry residues that are rich in fixed carbon (Panichkittikul et al. 2024). Materials obtained from agricultural wastes, industrial by-products and typical wastes can be used to remove impurities in sorption processes (Araujo et al. 2021). In addition to their low cost, carbonaceous materials exhibit high surface area and porosity and superior stability properties (Taylor et al. 2024). One way to best utilize biomass is to apply it as a precursor to the production of bio-based carbon porous materials (dos Reis et al. 2022).

Materials can be activated by applying physical and chemical processes (Tang et al. 2023). The chemical method involves treating the material with chemicals (Pereira et al. 2014). Although chemicals are used for this method, physical activation requires a long time and high temperature and energy needs (Yossa et al. 2020). Functional groups can be introduced by chemical treatment to ensure the affinity of materials to impurities in the aqueous environment (Gita et al. 2023). Moreover, chemical activation results in high carbon yield, large surface area and well-developed porous structure (Kılıç et al. 2012). Different reactions occur for different agents, as explained by Xing et al (Xing et al. 2019). Chemical agents cause strong cross-links through dehydration and elimination reactions, prevent volume shrinkage, provide high porosity and add functional groups to the material (Guo and Lua 2003). Chemical treatment agents can be acidic, alkaline and oxidizing agents, metal salts and a combination thereof (Zhang et al. 2023). Commonly used acidic activating agents are nitric acid, hydrochloric acid, sulfuric acid, and phosphoric acid (España et al. 2019).

Dyes are difficult to remove from wastewater because they are resistant to biological degradation (Zhu et al. 2014). The elimination of crystal violet, an alkaline dye, from industrial wastewater attracts attention in terms of water improvement (Gupta et al. 2023). It is used in many areas such as fabric dyeing, adhesive tapes, ink production, leather processing, food industry, fingerprint detection and veterinary medicine (Abd El-Hamid et al. 2022, Kumbhar et al. 2022). Since crystal violet is widely used as a dye with high economic value, it is mixed in effluents and therefore poses a health risk (Huang et al. 2023). It can be more toxic than many other types of dyes due to the production of dangerous aromatic amino products (Benhalima et al. 2023). Its complex structure makes it more toxic and dangerous than anionic dyes (Tan et al. 2023). Even very low concentrations (1 mg/L) threaten living life by negatively affecting light transmission to aquatic environments (Loganathan et al. 2022). Therefore, its effective removal from water is of great necessity (Wu et al. 2021).

In this study, it is aimed to determine the changes caused by different acidic agents in the properties of kiwi peels, to evaluate the effects of each acidic agent individually and to compare them with each other. In addition, the sorption performances provided by the properties that each acidic agent brings to the kiwi peels and the kinetics of the sorptions were investigated. In the literature, many different biomass such as algae (Kumar et al. 2016), green seaweed (Bertoni et al. 2015), soy hull (Blanes et al. 2016), flower (Lingamdinne et al. 2016), hickory chips, cotton stalks and peanut hulls (Ding et al. 2014), exhausted coffee (Liu et al. 2016), reed (Rawajfih and Nsour 2008) and hazelnut and almond shell (Pehlivan et al. 2009) have been used for sorption purposes. There have been studies involving kiwi peels in sorption processes, and it is noteworthy that these studies are current. Gubitosa et al. (2022) used kiwi peels as adsorbent for Ciprofloxacin removal. A Zn–Fe biochar (KB/Zn-Fe) was designed from a kiwi branch and used in Pb (II) removal from an aqueous solution by Tan et al. (2022a). There is a study in which chitosan-modified kiwi branch biochar was prepared for Cd (II) removal (Tan et al. 2022b). Gong et al. (2024) produced manganese dioxide-decorated kiwi peel powder for the removal of Pb^{2+}. Unlike previous studies, this study revealed the changes in the properties of kiwi peels with hydrochloric acid (HCl), sulfuric acid (H_2SO_4) and phosphoric acid (H_3PO_4). In addition, the effect of each agent on the crystal violet sorption performance of kiwi peels was investigated. In this way, the preparation of kiwi peels with a different method and the use of a different material for sorption than the studies on kiwi mentioned above demonstrates the innovative aspect of the study. The important points of the study that contribute to the studies in this field are that a detailed study is carried out by determining the effects of different agents for both characterization and sorption, that a wide scope is provided for the study by comparing various functionalizations, and that the study includes an easy process with common chemicals as a preparation method. In addition, according to the literature reviews above, the fact that the studies on kiwi are from recent years shows that studies on kiwi have intensified, and it is seen that this study carried out in this direction is currently remarkable.

2. Materials and Methods

2.1. Functionalization of Biomass

Kiwi fruits were purchased from a market in Bilecik. They were peeled and the peels were collected. It was left to dry for approximately 2 months in the presence of sunlight. The dried peels were broken and ground. It was then functionalized by HCl (≥37%, Honeywell Fluka), H_2SO_4 (95-97%, Honeywell Riedel-de Haen) and H_3PO_4 (orthophosphoric acid, 85%, Carlo Erba). Acidic agents were used without any treatment or dilution. Material preparation was carried out by chemical treatment similar to previous studies (Van Veenhuyzen et al. 2021, Almeida et al. 2021). 8 g of ground kiwi peel was placed in 60 mL of acid and stirred slowly for 2 h at 90°C for effective contact. Then, it was kept at 90°C for 2 h without mixing. Kiwi peels functionalized with acidic agents were washed several times with 0.5M sodium hydroxide (NaOH, Carlo Erba) solution. It was washed with distilled water and the pH was ensured to reach between 6-7. Kiwi peels were dried in an oven at 105°C. Raw kiwi peels were named KP, and kiwi peels prepared by functionalizing using HCl, H_2SO_4 and H_3PO_4 were called HAFKP, SAFKP and PAFKP, respectively.

2.2. Sorption

Sorption studies were carried out with kiwi peels prepared by functionalizing them with acidic agents. The sorption efficiency of HAFKP, SAFKP and PAFKP was investigated by preparing simulated wastewater containing crystal violet (Fluka) dye. Simulated wastewater was prepared at its own pH value and in a volume of 50 mL, containing dye at an initial concentration of 10 mg/L. A shaking water bath was used for the experiments. The experiments were repeated twice. Absorbance values of aqueous solutions including the dye were determined by Ultraviolet-Visible region (UV-Vis) spectroscopy at 590 nm wavelength and recorded. These values were converted to concentration values using the absorbance versus concentration curve prepared at different concentrations of the dye. The concentration values were used to calculate the sorption percentage and capacity given in Equations (1) and (2), respectively (Manzar et al. 2023):

$$\text{sorption } \% = \frac{(C_0 - C_e)}{C_0} x100 \quad (1)$$

$$q_t = \frac{(C_0 - C_t)\, V}{m} \quad (2)$$

C_0, C_e and C_t represent the initial, equilibrium and concentration values at any time t (mg L^{-1}), q_t indicates the sorption capacity (mg g^{-1}), V represents the solution volume (L), and m indicates the mass of the material (g), respectively (Manzar et al. 2023).

2.2.1. Kinetics

Kinetic studies were carried out to evaluate the processes in which HAFKP, SAFKP and PAFKP were used in sorption processes. The equations used are listed below (Cui et al. 2015, Berhane et al. 2017, Veneu et al. 2019):

Pseudo-first order kinetic model:

$$q_t = q_e(1 - e^{-k_1 t}) \quad (3)$$

Pseudo-second order kinetic model:

$$q_t = \frac{q_e^2 k_2 t}{1 + q_e k_2 t} \quad (4)$$

Elovich model: $q_t = \frac{1}{\beta} \ln(\beta\alpha t + 1)$ (5)

Bangham model: $q_t = k_3 t^{\alpha B}$ (6)

q_e indicates the amount retained in the solid at equilibrium (mg g^{-1}), and k_1 is the pseudo-first order reaction velocity constant (g mg^{-1} min^{-1}), t represents time (min), k_2 is the pseudo-second order reaction velocity constant (g mg^{-1} min^{-1}), α indicates the initial sorption rate constant (mg kg^{-1} min^{-1}), β indicates a sorption constant (kg mg^{-1}) and α β and k_3 are related constants for Bangham isotherm (Cui et al. 2015, Berhane et al. 2017, Veneu et al. 2019).

2.3. Apparatus

For KP, HAFKP, SAKKP and PAFKP, functional groups of raw kiwi peels and materials prepared depending on the changing agent were detected using Fourier transform infrared spectroscopy (FTIR). The X-ray diffraction (XRD) method was applied to investigate the amorphous or crystalline structure of functionalized kiwi peels. The surface morphologies of the materials were investigated and elemental composition of the surfaces was exhibited using scanning electron microscopy-energy dispersive X-ray spectroscopy (SEM-EDX).

3. Results and Discussion

3.1. Characteristics

The functional groups of KP, HAFKP, SAFKP and PAFKP were determined and the effective groups for dye sorption were analyzed. Figure 1(a), (b), (c) and (d) show the FTIR spectra of KP, HAFKP, SAFKP and PAFKP, respectively. The broad and distinct peak seen at 3293 cm^{-1} for KP in Figure 1(a) belongs to the vibrations of O-H groups,

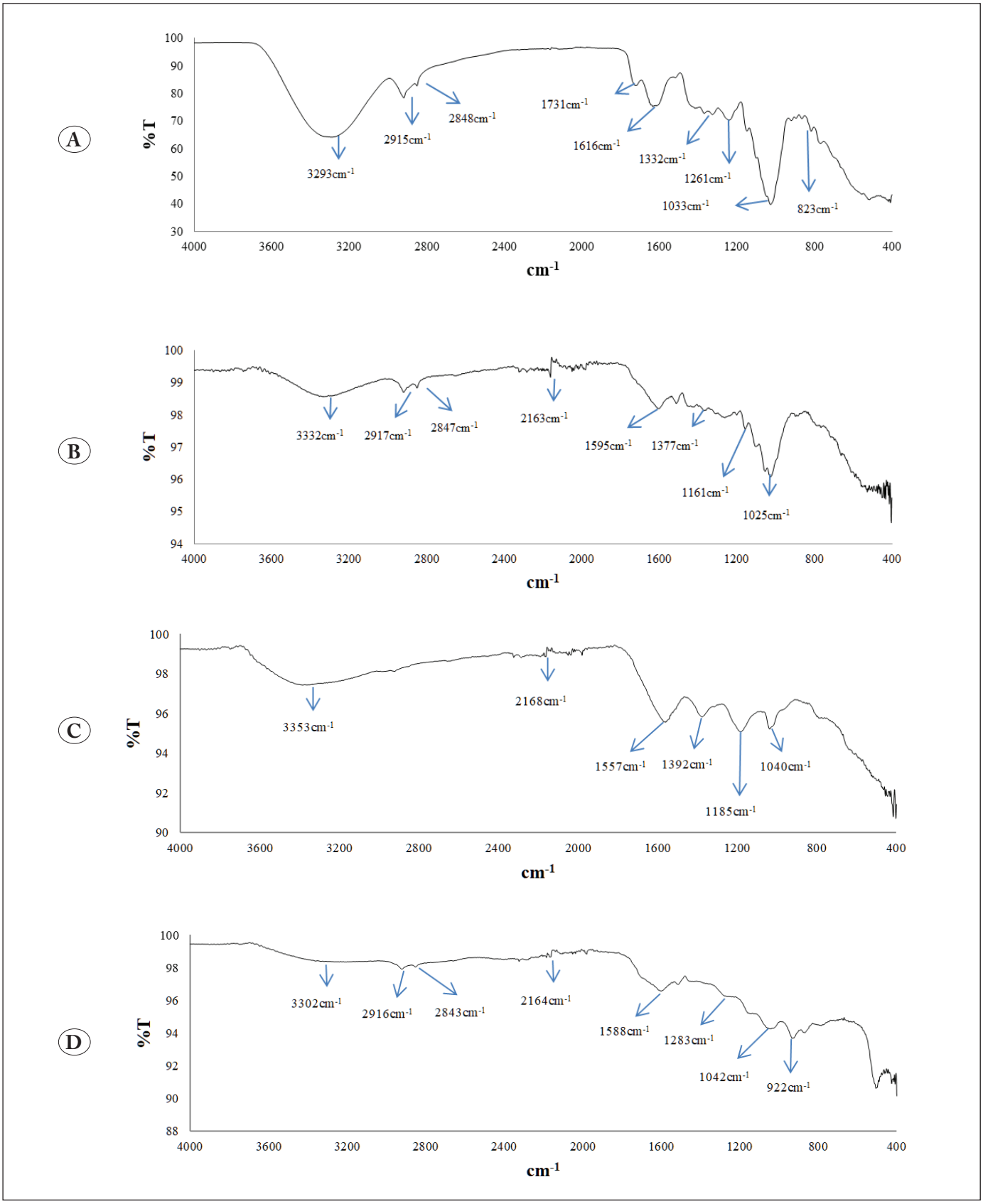

Figure 1. FTIR spectra of **(A)** KP, **(B)** HAFKP, **(C)** SAFKP, and **(D)** PAFKP.

however, its effect seems to have decreased, which may be due to the thermal treatment along with the functionalization at 3332, 3353 and 3302 cm^{-1} for HAFKP, SAFKP and PAFKP, respectively (Zbair et al. 2020, Adnan and Moses 2020, Hao et al. 2023, Tirkey and Babu 2024). The peaks that lose their effect for SAFKP and in the range of 2915-2917 and 2843-2848 cm^{-1} for other samples indicate CH_2 stretching vibrations (Kuracina et al. 2023, Stelescu et al. 2022). CO stretching peaks appeared in the range of 2163-2168 cm^{-1} in the materials prepared by functionalization of KP (Yang and Wöll 2017). KP has a C=O band according to 1731 and 1616 cm^{-1} (Phothong et al. 2024, B.Aziz et al. 2019). The peaks seen at 1595, 1557 and 1588 cm^{-1} for HAFKP, SAFKP and PAFKP may belong to C-H, C-N and -COOH vibrations, respectively (Gan and Tan 2001, Dutta et al. 2019, Yamada and Mizuno 2021). While the CH_3 bending peak was observed at 1377 cm^{-1} for HAFKP, C-O peaks were observed at 1332, 1392 and 1283 cm^{-1} for KP, SAFKP and PAFKP, respectively (Gupta et al. 2017, Jung et al. 2018, Rani et al. 2016, Rajaniverma et al. 2022). In Figure 1(a), a CH_3 bending peak was detected at 1261 cm^{-1} in KP (Guo et al. 2012). The peaks at 1185 (Figure 1(c)), 1161 (Figure 1(b)) and 1033 (Figure 1(a)) cm^{-1} indicate C-O vibrations (Nikafshar et al. 2017, Karabıyık et al. 2023, Bandyopadhyay et al. 2021). The 1042 cm^{-1} peak in Figure 1(d) may belong to P=O and P-O-P vibrations of PAFKP (Tang et al. 2019, Silva et al. 2021, Wu et al. 2023). For SAFKP, the peak at 1040 cm^{-1} may belong to the $-SO_2$ group (Figure 1(c)) (Wu et al. 2017). The 1025 cm^{-1} peak in Figure 1(b) indicates C-OH stretching vibrations (Zhang et al. 2022). The 922 cm^{-1} peak seen for PAFKP may belong to the presence of P (Mustafa et al. 2023). For KP, there is a C–O–C stretching vibration peak at 823 cm^{-1} (Abolins et al. 2020). Interactions of different elements may take place in the region below 800 cm^{-1} (Peng et al. 2023, Isaac et al. 2023, Jin et al. 2023).

XRD analysis was performed to determine whether HAFKP, SAFKP and PAFKP were amorphous or crystalline. Figure 2(a), (b) and (c) are the XRD diffractograms of HAFKP,

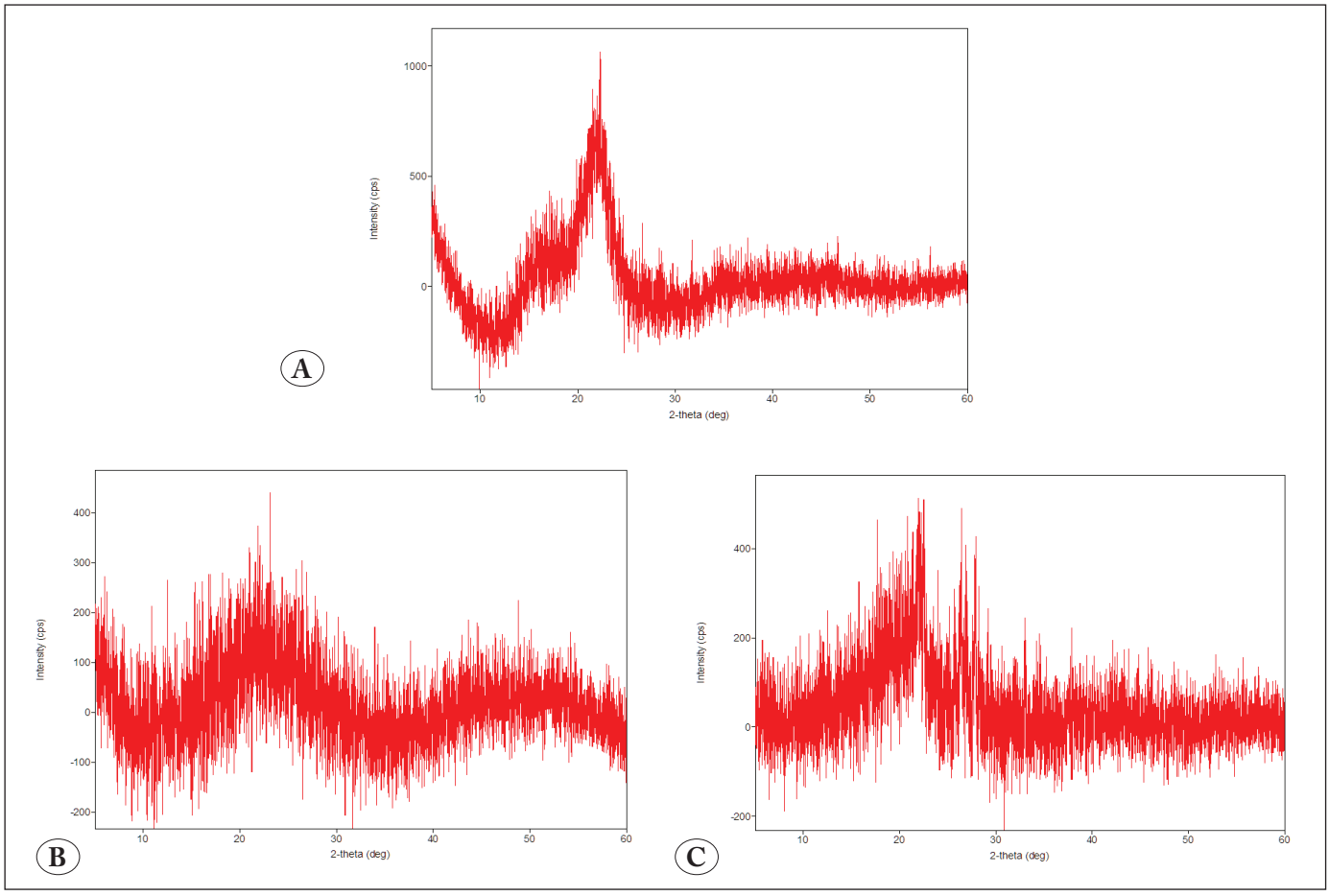

Figure 2. X-ray diffractograms of **(A)** HAFKP, **(B)** SAFKP, and **(C)** PAFKP.

SAFKP and PAFKP, respectively. According to Figure 2, peaks at similar 2θ values were observed for HAFKP, SAFKP and PAFKP. Similar to the study by Santos et al., HAFKP, SAFKP and PAFKP exhibited an amorphous structure with a small number of crystal patterns (Santos et al. 2023).

To monitor the changes in the surface structure of KP with functionalization, SEM analyzes were performed for HAFKP, SAFKP and PAFKP and these analyzes were compared with the SEM analyzes of KP. In the SEM images of KP at different magnifications in Figures 3(a) and (b), a non-porous, irregular and lumpy surface structure is seen, as in the study by Gubitosa et al. in which they examined the external and internal structure of the kiwi peel (Gubitosa et al. 2022). In the SEM images of HAFKP in Figure 3(c) and (d), it is clear that HCl causes the formation of irregular and crevice-shaped regions on the surface of KP. Similar to the previous study presented by Xing et al., it

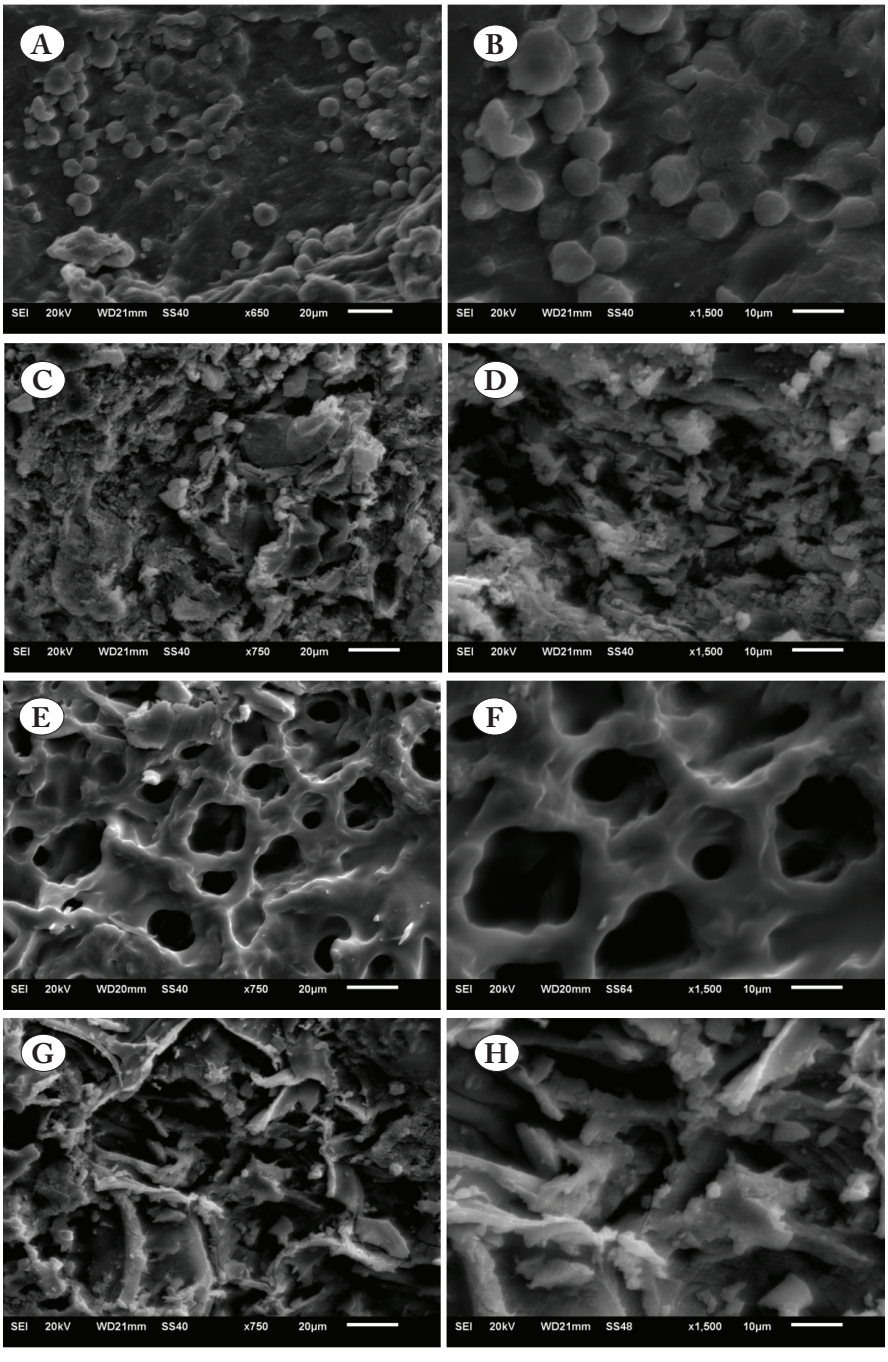

Figure 3. SEM images of KP **(A and B)**, HAFKP **(C and D)**, SAFKP **(E and F),** and PAFKP **(G and H)**.

resulted in a corrugated and layered surface structure on the KP surface with agglomerations with HCl (Xing et al. 2016). In Figure 3(e) and (f) of SAFKP, it is seen that H_2SO_4 causes the formation of a highly porous structure containing open pores of different sizes, as shown by Guo et al (Guo et al. 2023). In Figure 3(g) and (h) of PAFKP, an irregular surface with wide cracks is seen. Accordingly, it is seen that the surface structures change as a result of the functionalization of the raw material with acidic agents. In addition, it is clear in the SEM images in Figure 3 that different acidic agents change the surface structure of the raw material and cause surface structures of different shapes, sizes and distributions. These surface structures show that changes have been created on the surface of the non-porous KP by acidic functionalizations and that these structures of the newly prepared HAFKP, SAFKP and PAFKP may be suitable areas for sorption.

EDX analyzes were performed to examine the effect of different acids used for functionalization on the elemental composition on the surfaces of the materials. Figure 4(a), (b), (c) and (d) are EDX analyzes for KP, HAFKP, SAFKP and PAFKP, respectively. According to Figure 4(a), KP is a material with 21.5% O, 21.3% K, 16.1% Mg, 12.9% Zn and 11.6% Cu content by mass. For HCl applied HAFKP, 71.0% C, 11.4% O, 8.5% Cl and 5.5% Na content were determined (Figure 4(b)). SAFKP exhibited 57.9% C, 24.0% Na and 11.4% O content in Figure 4(c). The major elements for PAFKP were 47.1% C, 10.8% O and 10.5% Na (Figure 4(d)). According to EDX results, it was determined that the functionalization of kiwi peels with acidic chemical agents provided C content for HAFKP, SAFKP and PAFKP.

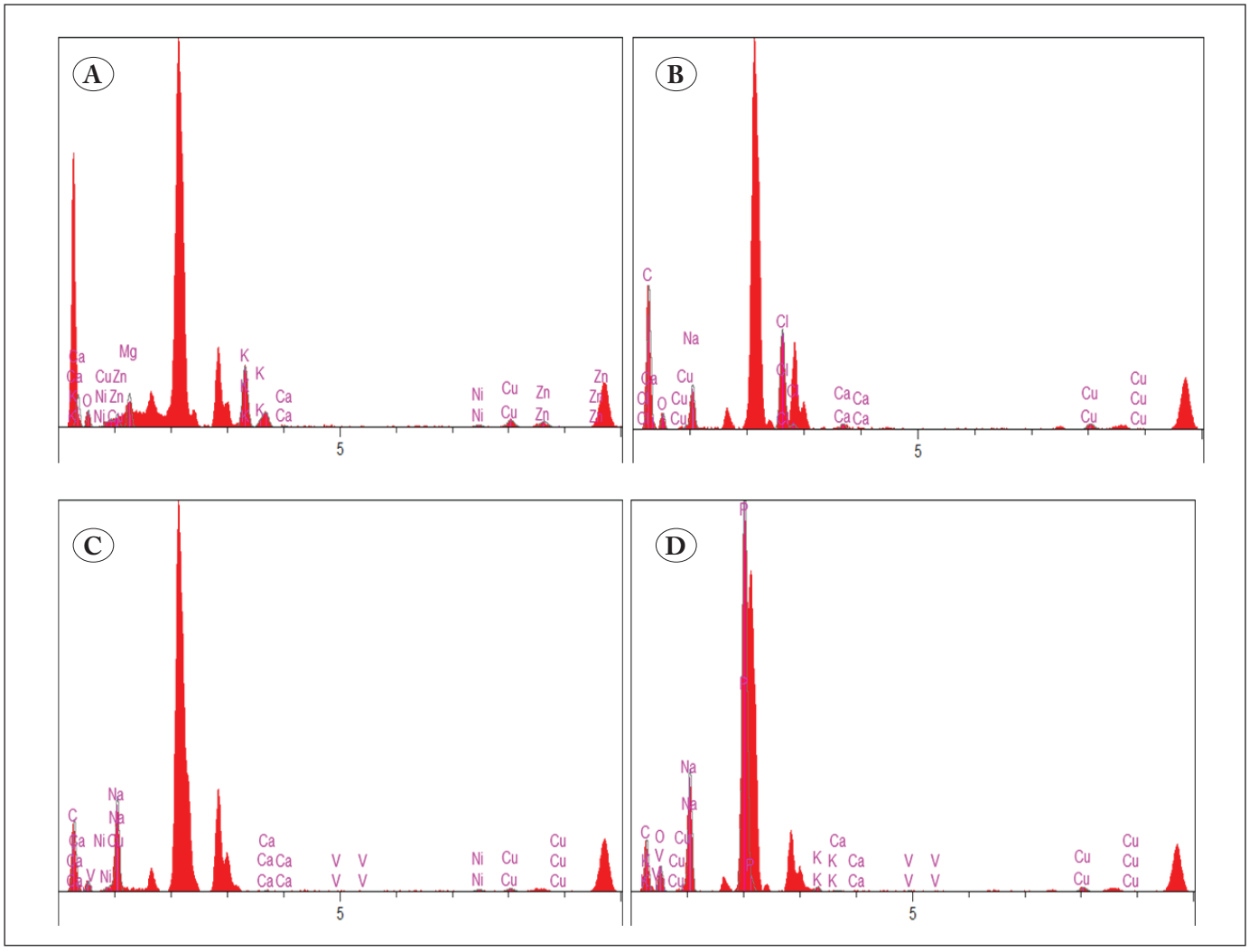

Figure 4. EDX analysis of **(A)** KP, **(B)** HAFKP, **(C)** SAFKP, and **(D)** PAFKP.

3.2. Sorption Analysis

3.2.1. Determination of sorption performance

The sorption performance of HAFKP, SAFKP and PAFKP over time is given in Figure 5(a), (b) and (c), respectively. For the experiments, the amount of material was determined as 0.1 g, the volume of the dye solution was 50 mL, the initial concentration of the dye solution was 10 mg/L, the pH value of the dye solution itself, the temperature was 24 °C and the shaking speed was 190 rpm. Under these conditions, concentration changes were monitored to determine the equilibrium times of the processes.

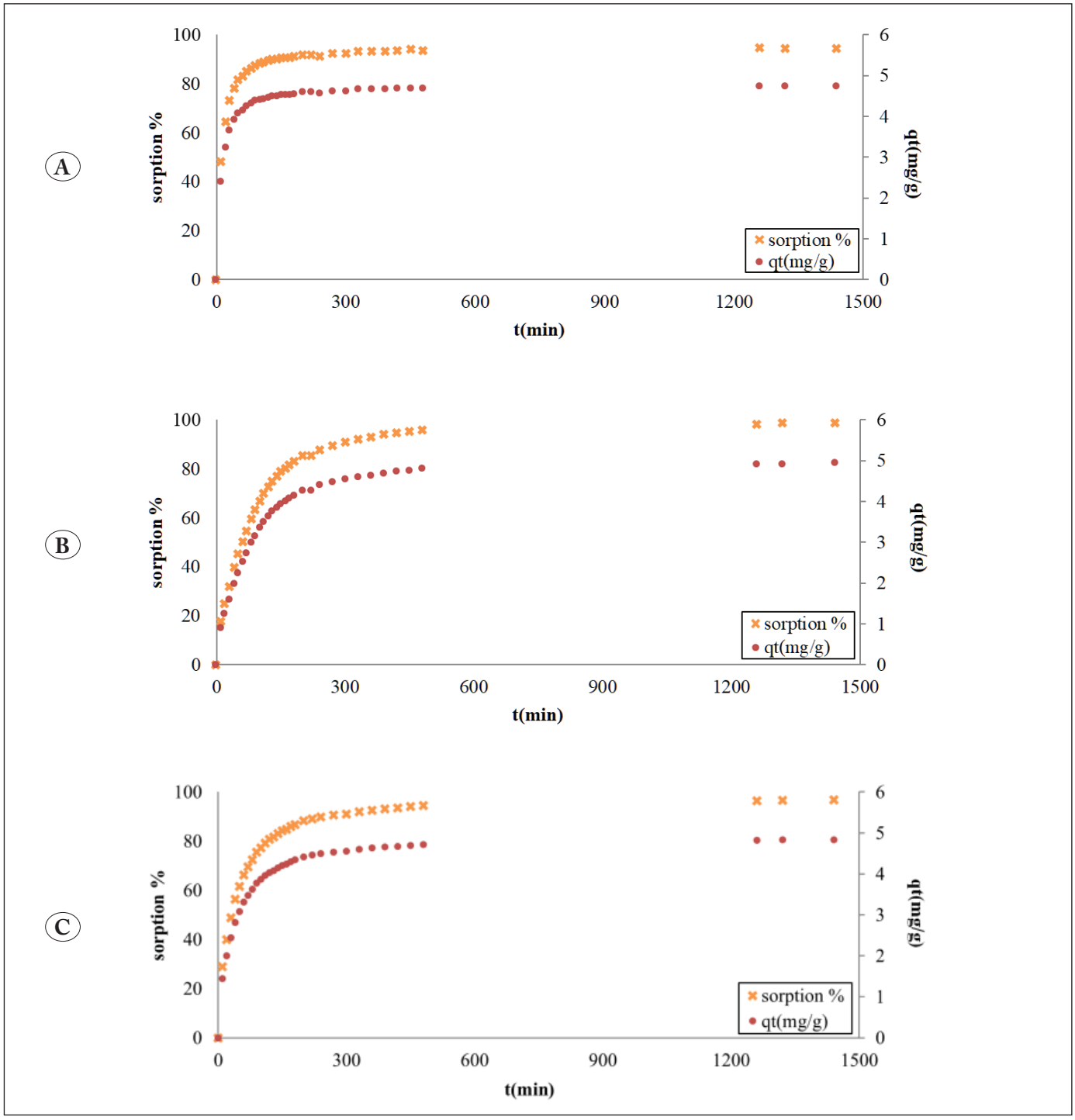

Figure 5. Sorption performance of **(A)** HAFKP, **(b)** SAFKP, and **(C)** PAFKP.

In the graph of HAFKP given in Figure 5(a), it is seen that high sorption is achieved (~50%) as soon as the experiment starts and this situation continues to increase rapidly until approximately 120 min. According to the figure, the increase continues after 120 min, but the rate of increase gradually decreases. A similar situation was observed for capacity values. When concentration changes were continued to be monitored to determine the equilibrium time, it was observed that the sorption performance increased with very small increases after 120 min. It was determined that the sorption performance of the process did not change due to the concentration value remaining constant at the end of 1440 min and therefore 1440 min was determined as the equilibrium time. When the performance of SAFKP was followed over time, Figure 5(b) was obtained. As seen in the figure, process performance increased over time at lower rates than HAFKP. The increasing trend, which started in the first moments of the experiment, continued for 480 min. Although the increases continued after 480 min, they remained at very low rates. 1440 min was chosen as the equilibrium time due to negligible increases at the end of 1440 min. This behavior caused the formation of the curve in Figure 5(b). However, similar to HAFKP, SAFKP also showed high performance at the end of 1440 min. Figure 5(c) shows the performance of PAFKP. PAFKP provided lower percent sorption values than HAFKP but higher than SAFKP in the first moments of the experiment. Although the stable sorption rates, which continued for 360 min, decreased after 360 min, PAFKP continued to perform. Similar to SAFKP, increases at the end of 1440 min were neglected and 1440 min was determined as the equilibrium time. Similar to HAFKP and SAFKP, PAFKP also exhibited high sorption performance at equilibrium time. At the end of 1440 min, HAFKP, SAFKP and PAFKP exhibited 94.53, 98.62 and 96.76% sorption and 4.73, 4.93 and 4.84 mg/g capacity, respectively. Although the sorption percentage and capacity values are very close to each other, the highest values were obtained for SAFKP.

3.2.2. Application of kinetic models to sorption

Kinetic studies were conducted to explain the performance of HAFKP, SAFKP and PAFKP. Kinetic studies for HAFKP, SAFKP and PAFKP using pseudo-first order, pseudo-second order, Elovich and Bangham models are plotted in Figure 6(a), (b) and (c), respectively.

The variables of the kinetic models are given in Table 1. According to the magnitude of the correlation coefficients (R^2) of the kinetic models in Table 1, pseudo-second order>pseudo-first order>Elovich>Bangham order was determined for HAFKP. For SAFKP, R^2 values increased in the order pseudo-first order>pseudo-second order>Elovich>Bangham. According to R^2 values, PAFKP showed a fit as pseudo-second order>pseudo-first order>Elovich>Bangham. The largest R^2 value for HAFKP and PAFKP was determined for the pseudo-second order kinetic model. Supporting this situation, the experimental q_e values were found to be close to the q_e values of the pseudo-second order

Table 1. Variables of kinetic models.

Model	Parameter	HAFKP	SAFKP	PAFKP
	experimental q_e	**4.73**	**4.93**	**4.84**
PFO	q_e	4.55	4.74	4.55
	k_1	0.058	0.012	0.022
	R^2	0.9129	0.9901	0.9481
PSO	q_e	4.79	5.38	5.00
	k_2	11.75	2.56	4.24
	R^2	0.9976	0.9891	0.9966
Elovich	α	349.19	0.28	1.41
	β	2.73	1.053	1.45
	R^2	0.7381	0.8922	0.8684
Bangham	αB	0.091	0.22	0.15
	k_3	2.73	1.18	1.80
	R^2	0.6651	0.7898	0.7793

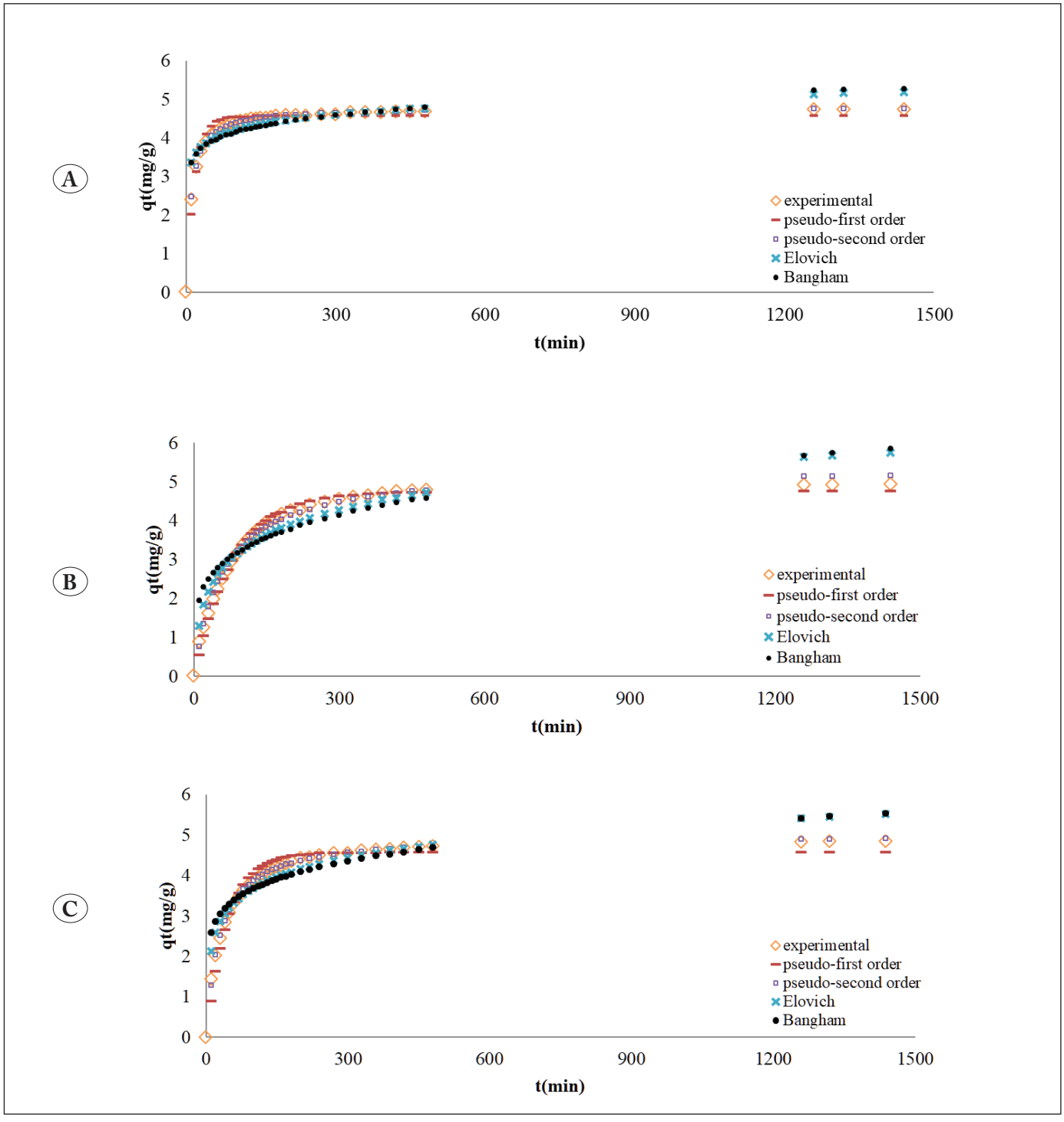

Figure 6. Experimental and kinetic model graphs of **(A)** HAFKP, **(B)** SAFKP and **(C)** PAFKP.

kinetic model for HAFKP and PAFKP. This model explains that chemisorption is the rate-determining step (Lammini et al. 2022). The fact that the processes for HAFKP and PAFKP are chemical sorption indicates that a chemical reaction occurs between the dye molecules and HAFKP and PAFKP, thus a strong bonding occurs through covalent bonds (Sasamoto et al. 2022). For SAFKP, although high and close R^2 values were obtained for both the pseudo-first order and pseudo-second order models, the R^2 value of the pseudo-first order was found to be higher with a very slight

difference. In addition, when the q_e values of the experimental and models are compared, the experimental qe value for SAFKP was found to be closer to the qe value for pseudo-first order. Therefore, it was determined that SAFKP and pseudo-first order kinetic model are compatible. Physical sorption is effective in processes suitable for the pseudo-first order kinetic model (Yin et al. 2023). Therefore, in the process involving SAFKP, sorption occurs physically. Physical sorption refers to processes that involve a reversible interaction through weak van der Waals forces (Atif et al. 2022). Therefore, it can be explained that SAFKP has a physical interaction with dye molecules. The Elovich model refers to the heterogeneous material surface when it comes to chemical sorption (Dinh et al. 2023). Bangham model describes diffusion into pores (Rojas et al. 2019). According to R^2 values, the processes carried out with HAFKP, SAFKP and PAFKP were not found to be compatible with the Elovich and Bangham model.

4. Conclusion

In this study, kiwi fruit peels were functionalized with different acidic agents and the properties of the resulting materials were determined. FTIR analysis showed that different acidic agents impart different functional groups to kiwi peel. The amorphous structure of the functionalized materials was revealed by XRD analysis. SEM analysis revealed that KP, which has a non-porous and non-homogeneous surface, exhibited open, large and circular pores when functionalized with H_2SO_4, while pores in the form of slits were formed for HAFKP and PAFKP. EDX analysis detected that acidic agents increase the C content in the elemental composition of the materials. Additionally, sorption performances of HAFKP, SAFKP and PAFKP were investigated. HAFKP, SAFKP and PAFKP exhibited crystal violet sorption performance of 94.53, 98.62 and 96.76%, respectively. In the kinetic analyzes applied for the processes, it was determined that the R^2 and q_e values of the processes in which HAFKP and PAFKP were used were compatible with the pseudo-second order kinetic model, and therefore, a strong bonding occurred between HAFKP and PAFKP and the dye molecules through covalent bonds. On the other hand, SAFKP was suitable for the pseudo-first order kinetic model and it was explained that sorption occurred with weaker binding.

5. Acknowledgements

The author received no funding for the research.

Conflict of Interest

The author declares that no conflict of interest.

6. References

Abd El-Hamid, HT., AlProl, AE., Hafiz, MA. 2022. The efficiency of adsorption modelling and Plackett-Burman design for remediation of crystal violet by *Sargassum latifolium*. Biocatalysis and Agricultural Biotechnology, 44: 102459. Doi: 10.1016/j.bcab.2022.102459

Abolins, A., Kirpluks, M., Vanags, E., Fridrihsone, A., Cabulis, U. 2020. Tall oil fatty acid epoxidation using homogenous and heterogeneous phase catalysts. Journal of Polymers and the Environment, 28: 1822-1831. Doi: 10.1007/s10924-020-01724-9

Adnan, M., Moses, J. 2020. A study on the thermophysiological and tactile comfort properties of silk/lyocell blended fabrics. Matéria (Rio de Janeiro), 25: e-12796. Doi: 10.1590/S1517-707620200003.1096

Almeida, ACM., do Nascimento, RA., Amador, ICB., de Sousa Santos, TC., Martelli, MC., de Faria, LJG., da Paixão Ribeiro, NF. 2021. Chemically activated red mud: assessing structural modifications and optimizing adsorption properties for hexavalent chromium. Colloids and Surfaces A: Physicochemical and Engineering Aspects, 628: 127325. Doi: 10.1016/j.colsurfa.2021.127325

Araujo, LA., Bezerra, CO., Cusioli, LF., Rodríguez, MT., Gomes, RG., Bergamasco, R. 2021. Diclofenac adsorption using a low-cost adsorbent derived from Guazuma ulmifolia Lam. fruit via chemical and thermal treatment. Journal of Environmental Chemical Engineering, 9(6): 106629. Doi: 10.1016/j.jece.2021.106629

Atif, M., Haider, HZ., Bongiovanni, R., Fayyaz, M., Razzaq, T., Gul, S. 2022. Physisorption and chemisorption trends in surface modification of carbon black. Surfaces and Interfaces, 31: 102080. Doi: 10.1016/j.surfin.2022.102080

Aziz, BS., Hussein, G., Brza, MA., Mohammed, JS., Abdulwahid, TR., Raza Saeed, S., Hassanzadeh, A. 2019. Fabrication of interconnected plasmonic spherical silver nanoparticles with enhanced localized surface plasmon resonance (LSPR) peaks using quince leaf extract solution. Nanomaterials, 9(11): 1557. Doi: 10.3390/nano9111557

Bandyopadhyay, S., Sáha, T., Sanétrník, D., Saha, N., Sáha, P. 2021. Thermo compression of thermoplastic Agar-Xanthan gum-carboxymethyl cellulose blend. Polymers, 13(20): 3472. Doi: 10.3390/polym13203472

Benhalima, T., Chicha, W., Ferfera-Harrar, H. 2023. Sponge-like biodegradable polypyrrole-modified biopolymers for selective adsorption of basic red 46 and crystal violet dyes from single and binary component systems. International Journal of Biological Macromolecules, 253: 127532. Doi: 10.1016/j.ijbiomac.2023.127532

Berhane, TM., Levy, J., Krekeler, MP., Danielson, ND. 2017. Kinetic sorption of contaminants of emerging concern by a palygorskite-montmorillonite filter medium. Chemosphere, 176: 231-242. Doi: 10.1016/j.chemosphere.2017.02.068

Bertoni, FA., Medeot, AC., González, JC., Sala, LF., Bellú, SE. 2015. Application of green seaweed biomass for MoVI sorption from contaminated waters. Kinetic, thermodynamic and continuous sorption studies. Journal of colloid and interface science, 446: 122-132. Doi: 10.1016/j.jcis.2015.01.033

Blanes, PS., Bordoni, ME., González, JC., García, SI., Atria, AM., Sala, LF., Bellú, SE. 2016. Application of soy hull biomass in removal of Cr (VI) from contaminated waters. Kinetic, thermodynamic and continuous sorption studies. Journal of environmental chemical engineering, 4(1): 516-526. Doi: 10.1016/j.jece.2015.12.008

Cui, L., Guo, X., Wei, Q., Wang, Y., Gao, L., Yan, L., Yan, T., Du, B. 2015. Removal of mercury and methylene blue from aqueous solution by xanthate functionalized magnetic graphene oxide: sorption kinetic and uptake mechanism. Journal of colloid and interface science, 439: 112-120. Doi: 10.1016/j.jcis.2014.10.019

Ding, Z., Hu, X., Zimmerman, AR., Gao, B. 2014. Sorption and cosorption of lead (II) and methylene blue on chemically modified biomass. Bioresource technology, 167: 569-573. Doi: 10.1016/j.biortech.2014.06.043

Dinh, LX., Van Tung, N., Lien, NT., Minh, PT., Le, TH. 2023. The Adsorption Kinetic and Isotherm Studies of Metal Ions (Co2+, Sr2+, Cs+) on Fe3O4 Nanoparticle of Radioactive Importance. Results in Chemistry, 6: 101095. Doi: 10.1016/j.rechem.2023.101095

dos Reis, GS., Guy, M., Mathieu, M., Jebrane, M., Lima, EC., Thyrel, M., Dotto, GL., Larsson, SH. 2022. A comparative study of chemical treatment by MgCl2, ZnSO4, ZnCl2, and KOH on physicochemical properties and acetaminophen adsorption performance of biobased porous materials from tree bark residues. Colloids and Surfaces A: Physicochemical and Engineering Aspects, 642: 128626. Doi: 10.1016/j.colsurfa.2022.128626

Dutta, R., Rao, MN., Kumar, A. 2019. Investigation of ionic liquid interaction with ZnBDC-metal organic framework through scanning EXAFS and inelastic neutron scattering. Scientific Reports, 9(1): 14741. Doi: 10.1038/s41598-019-51344-0

España, VAA., Sarkar, B., Biswas, B., Rusmin, R., Naidu, R. 2019. Environmental applications of thermally modified and acid activated clay minerals: Current status of the art. Environmental Technology & Innovation, 13: 383-397. Doi: 10.1016/j.eti.2016.11.005

Gan, SN., Tan, BY. 2001. FTIR studies of the curing reactions of palm oil alkyd–melamine enamels. Journal of Applied Polymer Science, 80(12): 2309-2315. Doi: 10.1002/app.1336

Gita, S., Shukla, SP., Deshmukhe, G., Singh, AR., Choudhury, TG. 2023. Adsorption linked fungal degradation process for complete removal of Lanasyn olive dye using chemically valorized sugarcane bagasse. Waste Management Bulletin, 1(1): 29-38. Doi: 10.1016/j.wmb.2023.04.002

Gong, H., Cao, Y., Zeng, W., Sun, C., Wang, Y., Su, J., Ren, H., Wang, P., Zhou, L., Kai, G., Qian, J. 2024. Manganese dioxide decorated kiwi peel powder for efficient removal of lead from aqueous solutions, blood and Traditional Chinese Medicine extracts. Environmental Research, 249: 118360. Doi: 10.1016/j.envres.2024.118360

Gubitosa, J., Rizzi, V., Cignolo, D., Fini, P., Fanelli, F., Cosma, P. 2022. From agricultural wastes to a resource: Kiwi Peels, as long-lasting, recyclable adsorbent, to remove emerging pollutants from water. The case of Ciprofloxacin removal. Sustainable Chemistry and Pharmacy, 29: 100749. Doi: 10.1016/j.scp.2022.100749

Guo, J., Lua, AC. 2003. Surface functional groups on oil-palm-shell adsorbents prepared by H3PO4 and KOH activation and their effects on adsorptive capacity. Chemical Engineering Research and Design, 81(5): 585-590. Doi: 10.1205/026387603765444537

Guo, F., Schulte, L., Vigild, ME., Ndoni, S. 2012. Load–release of small and macromolecules from elastomers with reversible gyroid mesoporosity. Soft Matter, 8(45): 11499-11507. Doi: 10.1039/C2SM26480C

Guo, Z., Fan, Y., Liu, T., Zhang, Y., Wan, Q. 2023. Adsorption and enrichment of Ag (I) from industrial wastewater using woody biomass-based biosorbent. Hydrometallurgy, 219: 106083. Doi: 10.1016/j.hydromet.2023.106083

Gupta, A., Lakshmp, YN., Manivannan, R., Victoria, SN. 2017. Visible range photocatalysts for solid phase photocatalytic degradation of polyethylene and polyvinyl chloride. Journal of the Chilean Chemical Society, 62(1): 3393-3398. Doi: 10.4067/S0717-97072017000100018

Gupta, S., Prajapati, A., Kumar, A., Acharya, S. 2023. Synthesis of silica aerogel and its application for removal of crystal violet dye by adsorption. Watershed Ecology and the Environment, 5: 241-254. Doi: 10.1016/j.wsee.2023.10.003

Hao, J., Chen, Y., Zhu, M., Zhao, Y., Zhang, K., Xu, X. 2023. Spatial-Temporal Heterogeneity in Large Three-Dimensional Nanofibrillar Cellulose Hydrogel for Human Pluripotent Stem Cell Culture. Gels, 9(4): 324. Doi: 10.3390/gels9040324

Huang, YP., Niu, HB., Jin, L., Jiao, L., Johnson, D., Tian, HL., Sarina, S., Zhu, HY., Fang, YF. 2023. Selective adsorption of Crystal Violet via hydrogen bonded water bridges by InVO4. Chemical Engineering Journal Advances, 15: 100508. Doi: 10.1016/j.ceja.2023.100508

Isaac, R., Siddiqui, S., Aldosari, OF., Uddin, MK. 2023. Magnetic biochar derived from Juglans regia for the adsorption of Cu2+ and Ni2+: Characterization, modelling, optimization, and cost analysis. Journal of Saudi Chemical Society, 27(6): 101749. Doi: 10.1016/j.jscs.2023.101749

Jin, Y., Liu, F., Li, Y., Du, Q., Song, F., Chen, B., Chen, K., Zhang, Y., Wang, M., Sun, Y., Zhao, S., Jing, Z., Pi, X., Wang, Y., Wang, D. 2023. Efficient adsorption of azo anionic dye Congo Red by micro-nano metal-organic framework MIL-68 (Fe) and MIL-68 (Fe)/chitosan composite sponge: preparation, characterization and adsorption performance. International Journal of Biological Macromolecules, 252: 126198. Doi: 10.1016/j.ijbiomac.2023.126198

Jung, MR., Horgen, FD., Orski, SV., Rodriguez, V., Beers, KL., Balazs, GH., Jones, TT., Work, TM., Brignac, KC., Royer, SJ., Hyrenbach, KD., Jensen, BA., Lynch, JM. 2018. Validation of ATR FT-IR to identify polymers of plastic marine debris, including those ingested by marine organisms. Marine pollution bulletin, 127: 704-716. Doi: 10.1016/j.marpolbul.2017.12.061

Karabıyık, M., Cihanoğlu, G., Ebil, Ö. 2023. CVD deposited epoxy copolymers as protective coatings for optical surfaces. Polymers, 15(3): 652. Doi: 10.3390/polym15030652

Kılıç, M., Apaydın-Varol, E., Pütün, AE. 2012. Preparation and surface characterization of activated carbons from Euphorbia rigida by chemical activation with ZnCl2, K2CO3, NaOH and H3PO4. Applied surface science, 261: 247-254. Doi: 10.1016/j.apsusc.2012.07.155

Kumar, D., Pandey, LK., Gaur, JP. 2016. Metal sorption by algal biomass: From batch to continuous system. Algal research, 18: 95-109. Doi: 10.1016/j.algal.2016.05.026

Kumbhar, P., Narale, D., Bhosale, R., Jambhale, C., Kim, JH., Kolekar, S. 2022. Synthesis of tea waste/Fe3O4 magnetic composite (TWMC) for efficient adsorption of crystal violet dye: Isotherm, kinetic and thermodynamic studies. Journal of Environmental Chemical Engineering, 10(3): 107893. Doi: 10.1016/j.jece.2022.107893

Kuracina, R., Szabová, Z., Buranská, E., Kosár, L., Rantuch, P., Blinová, L., Měřínská, D., Gogola, P., Jurina, F. 2023. Study into the fire and explosion characteristics of polymer powders used in engineering production technologies. Polymers, 15(21): 4203. Doi: 10.3390/polym15214203

Lammini, A., Dehbi, A., Omari, H., ELazhari, K., Mehanned, S., Bengamra, Y., Dehmani, Y., Rachid, O., Alrashdi, AA., Gotore, O., Abdellaoui, A., Lgaz, H. 2022. Experimental and theoretical evaluation of synthetized cobalt oxide for phenol adsorption: Adsorption isotherms, kinetics, and thermodynamic studies. Arabian Journal of Chemistry, 15(12): 104364. Doi: 10.1016/j.arabjc.2022.104364

Lingamdinne, LP., Yang, JK., Chang, YY., Koduru, JR. 2016. Low-cost magnetized Lonicera japonica flower biomass for the sorption removal of heavy metals. Hydrometallurgy, 165: 81-89. Doi: 10.1016/j.hydromet.2015.10.022

Liu, C., Fiol, N., Villaescusa, I., Poch, J. 2016. New approach in modeling Cr (VI) sorption onto biomass from metal binary mixtures solutions. Science of The Total Environment, 541: 101-108. Doi: 10.1016/j.scitotenv.2015.09.020

Loganathan, M., Raj, AS., Murugesan, A., Kumar, PS. 2022. Effective adsorption of crystal violet onto aromatic polyimides: Kinetics and isotherm studies. Chemosphere, 304: 135332. Doi: 10.1016/j.chemosphere.2022.135332

Manzar, MS., Aziz, HA., Meili, L., Ihsanullah, I., Palaniandy, P., Al-Harthi, MA. 2023. Insights into the adsorption of tetracycline onto cellulose nanocrystal structured MgAl/LDH composite. Materials Chemistry and Physics, 299: 127247. Doi: 10.1016/j.matchemphys.2022.127247

Mustafa, MN., Abdah, MAAM., Numan, A., Sulaiman, Y., Walvekar, R., Khalid, M. 2023. Development of high-performance MXene/nickel cobalt phosphate nanocomposite for electrochromic energy storage system using response surface methodology. Journal of Energy Storage, 68: 107880. Doi: 10.1016/j.est.2023.107880

Nikafshar, S., Zabihi, O., Hamidi, S., Moradi, Y., Barzegar, S., Ahmadi, M., Naebe, M. 2017. A renewable bio-based epoxy resin with improved mechanical performance that can compete with DGEBA. RSC advances, 7(14): 8694-8701. Doi: 10.1039/C6RA27283E

Panichkittikul, N., Mariyappan, V., Wu, W., Patcharavorachot, Y. 2024. Improvement of biohydrogen production from biomass using supercritical water gasification and CaO adsorption. Fuel, 361: 130724. Doi: 10.1016/j.fuel.2023.130724

Pehlivan, E., Altun, T., Cetin, S., Bhanger, MI. 2009. Lead sorption by waste biomass of hazelnut and almond shell. Journal of hazardous materials, 167(1-3): 1203-1208. Doi: 10.1016/j.jhazmat.2009.01.126

Peng, SY., Lin, YW., Lin, YY., Lin, KL. 2023. Hydrothermal synthesis of hydroxyapatite nanocrystals from calcium-rich limestone sludge waste: Preparation, characterization, and application for Pb2+ adsorption in aqueous solution. Inorganic Chemistry Communications, 160: 111943. Doi: 10.1016/j.inoche.2023.111943

Pereira, RG., Veloso, CM., da Silva, NM., de Sousa, LF., Bonomo, RCF., de Souza, AO., da Guarda Souza, MO., Fontan, RDCI. 2014. Preparation of activated carbons from cocoa shells and siriguela seeds using H3PO4 and ZnCL2 as activating agents for BSA and α-lactalbumin adsorption. Fuel Processing Technology, 126: 476-486. Doi: 10.1016/j.fuproc.2014.06.001

Phothong, N., Boontip, T., Chouwatat, P., Aht-Ong, D., Napathorn, SC. 2024. Preparation and characterization of astaxanthin-loaded biodegradable polyhydroxybutyrate (PHB) microbeads for personal care and cosmetic applications. International Journal of Biological Macromolecules, 257: 128709. Doi: 10.1016/j.ijbiomac.2023.128709

Rajaniverma, D., Rao, DJ., Prasanna Kumar, PV., Seetaramaiah, V., Ramakrishna, Y. 2022. Characterization of Structure-Property Relations and Second Harmonic Generation of 6-Methoxy-2-Naphthaldehyde. Polycyclic Aromatic Compounds, 42(8): 5796-5808. Doi: 10.1080/10406638.2021.1956553

Rani, S., Kumar, M., Garg, R., Sharma, S., Kumar, D. 2016. Amide functionalized graphene oxide thin films for hydrogen sulfide gas sensing applications. IEEE Sensors Journal, 16(9): 2929-2934. Doi: 10.1109/JSEN.2016.2524204

Rawajfih, Z., Nsour, N. 2008. Thermodynamic analysis of sorption isotherms of chromium (VI) anionic species on reed biomass. The Journal of Chemical Thermodynamics, 40(5): 846-851. Doi: 10.1016/j.jct.2008.01.005

Rojas, J., Suarez, D., Moreno, A., Silva-Agredo, J., Torres-Palma, RA. 2019. Kinetics, isotherms and thermodynamic modeling of liquid phase adsorption of crystal violet dye onto shrimp-waste in its raw, pyrolyzed material and activated charcoals. Applied Sciences, 9(24): 5337. Doi: 10.3390/app9245337

Santos, NC., Almeida, RLJ., Saraiva, MMT., de Alcântara Ribeiro, VH., De Sousa, FM., De Lima, TLB., de Alcântara Silva, VM., André, AMMCN., Leite Filho, MT., de Almeida Mota, MM. 2023. Application of microwave-assisted freeze–thaw pretreatment in kiwi drying: mass transfer, X-ray diffraction and bioaccessibility of phenolic compounds. Journal of Food Measurement and Characterization, 17(4): 3523-3533. Doi: 10.1007/s11694-023-01895-8

Sasamoto, R., Kanda, Y., Yamanaka, S. 2022. Difference in cadmium chemisorption on calcite and vaterite porous particles. Chemosphere, 297: 134057. Doi: 10.1016/j.chemosphere.2022.134057

Silva, MC., Spessato, L., Silva, TL., Lopes, GK., Zanella, HG., Yokoyama, JT., Cazetta, AL., Almeida, VC. 2021. H3PO4–activated carbon fibers of high surface area from banana tree pseudo-stem fibers: adsorption studies of methylene blue dye in batch and fixed bed systems. Journal of Molecular Liquids, 324: 114771. Doi: 10.1016/j.molliq.2020.114771

Stelescu, MD., Sonmez, M., Alexandrescu, L., Nituica, M., Gurau, DF., Georgescu, M. 2022. Structure and properties of blends based on vulcanized rubber waste and styrene–butadiene–styrene thermoplastic elastomer. Journal of Rubber Research, 25(5): 421-434. Doi: 10.1007/s42464-022-00187-y

Tan, Q., Jia, X., Dai, R., Chang, H., Woo, MW., Chen, H. 2023. Synthesis of a novel magnetically recyclable starch-based adsorbent for efficient adsorption of crystal violet dye. Separation and Purification Technology, 320: 124157. Doi: 10.1016/j.seppur.2023.124157

Tan, Y., Wan, X., Zhou, T., Wang, L., Yin, X., Ma, A., Wang, N. 2022a. Novel Zn-Fe engineered kiwi branch biochar for the removal of Pb (II) from aqueous solution. Journal of Hazardous Materials, 424: 127349. Doi: 10.1016/j.jhazmat.2021.127349

Tan, Y., Wan, X., Ni, X., Wang, L., Zhou, T., Sun, H., Wang, N., Yin, X. 2022b. Efficient removal of Cd (II) from aqueous solution by chitosan modified kiwi branch biochar. Chemosphere, 289: 133251. Doi: 10.1016/j.chemosphere.2021.133251

Tang, Y., Zhao, Y., Lin, T., Li, Y., Zhou, R., Peng, Y. 2019. Adsorption performance and mechanism of methylene blue by H3PO4-modified corn stalks. Journal of Environmental Chemical Engineering, 7(6): 103398. Doi: 10.1016/j.jece.2019.103398

Tang, Z., Gao, J., Zhang, Y., Du, Q., Feng, D., Dong, H., Peng, Y., Zhang, T., Xie, M. 2023. Ultra-microporous biochar-based carbon adsorbents by a facile chemical activation strategy for high-performance CO2 adsorption. Fuel Processing Technology, 241: 107613. Doi: 10.1016/j.fuproc.2022.107613

Taylor, JH., Troisi, G., Soltani, SM. 2024. Application of chemically-activated recycled carbon fibres for aqueous-phase adsorptions-part I: Optimisation of activation process. Chemical Engineering Journal Advances, 18: 100591. Doi: 10.1016/j.ceja.2024.100591

Tirkey, A., Babu, PJ. 2024. Synthesis and characterization of citrate-capped gold nanoparticles and their application in selective detection of creatinine (A kidney biomarker). Sensors International, 5: 100252. Doi: 10.1016/j.sintl.2023.100252

Van Veenhuyzen, B., Tichapondwa, S., Hörstmann, C., Chirwa, E., Brink, HG. 2021. High capacity Pb (II) adsorption characteristics onto raw-and chemically activated waste activated sludge. Journal of Hazardous Materials, 416: 125943. Doi: 10.1016/j.jhazmat.2021.125943

Veneu, DM., Yokoyama, L., Cunha, OGC., Schneider, CL., de Mello Monte, MB. 2019. Nickel sorption using Bioclastic Granules as a sorbent material: equilibrium, kinetic and characterization studies. Journal of Materials Research and Technology, 8(1): 840-852. Doi: 10.1016/j.jmrt.2018.05.020

Wu, Q., Wei, J., Xu, B., Liu, X., Wang, H., Wang, W., Wang, Q., Liu, W. 2017. A robust, highly stretchable supramolecular polymer conductive hydrogel with self-healability and thermo-processability. Scientific reports, 7(1): 41566. Doi: 10.1038/srep41566

Wu, Z., Deng, W., Tang, S., Ruiz-Hitzky, E., Luo, J., Wang, X. 2021. Pod-inspired MXene/porous carbon microspheres with ultrahigh adsorption capacity towards crystal violet. Chemical Engineering Journal, 426: 130776. Doi: 10.1016/j.cej.2021.130776

Wu, Z., Chen, Z., Tang, J., Zhou, Z., Chen, L., Fang, Y., Hu, X., Lv, J. 2023. Efficient adsorption and reduction of Cr (VI) in water using one-step H3PO4-assisted prepared Leersia hexandra Swartz hydrochar. Materials Today Sustainability, 21: 100260. Doi: 10.1016/j.mtsust.2022.100260

Xing, Z., Ju, Z., Zhao, Y., Wan, J., Zhu, Y., Qiang, Y., Qian, Y. 2016. One-pot hydrothermal synthesis of Nitrogen-doped graphene as high-performance anode materials for lithium ion batteries. Scientific reports, 6(1): 26146. Doi: 10.1038/srep26146

Xing, X., Jiang, W., Li, S., Zhang, X., Wang, W. 2019. Preparation and analysis of straw activated carbon synergetic catalyzed by ZnCl2-H3PO4 through hydrothermal carbonization combined with ultrasonic assisted immersion pyrolysis. Waste Management, 89: 64-72. Doi: 10.1016/j.wasman.2019.04.002

Yamada, T., Mizuno, M. 2021. Infrared Spectroscopy in the Middle Frequency Range for Various Imidazolium Ionic Liquids—Common Spectroscopic Characteristics of Vibrational Modes with In-Plane+ C (2)–H and+ C (4, 5)–H Bending Motions and Peak Splitting Behavior Due to Local Symmetry Breaking of Vibrational Modes of the Tetrafluoroborate Anion. ACS omega, 6(2): 1709-1717. Doi: 10.1021/acsomega.0c05769

Yang, C., Wöll, C. 2017. IR spectroscopy applied to metal oxide surfaces: adsorbate vibrations and beyond. Advances in Physics: X, 2(2): 373-408. Doi: 10.1080/23746149.2017.1296372

Yin, H., Xiong, Q., Zhang, M., Wang, B., Zhang, F. 2023. Multi-principles analysis of Cu (II) adsorption in water on magnetic microspheres and modified Chitosan. Journal of Environmental Chemical Engineering, 11(6): 111285. Doi: 10.1016/j.jece.2023.111285

Yossa, LN., Ouiminga, SK., Sidibe, SS., Ouedraogo, IWK. 2020. Synthesis of a cleaner potassium hydroxide-activated carbon from baobab seeds hulls and investigation of adsorption mechanisms for diuron: Chemical activation as alternative route for preparation of activated carbon from baobab seeds hulls and adsorption of diuron. Scientific African, 9: e00476. Doi: 10.1016/j.sciaf.2020.e00476

Zbair, M., Bottlinger, M., Ainassaari, K., Ojala, S., Stein, O., Keiski, RL., Bensitel, M., Brahmi, R. 2020. Hydrothermal carbonization of argan nut shell: functional mesoporous carbon with excellent performance in the adsorption of bisphenol A and diuron. Waste and biomass valorization, 11: 1565-1584. Doi: 10.1007/s12649-018-00554-0

Zhang, M., Ding, R., Hu, F. 2022. Comparison on FTIR spectrum and thermal analysis for four types of Rehamnnia glutinosa and their extracts. Doi: 10.21203/rs.3.rs-1319441/v1

Zhang, Y., Zhang, J., Chen, K., Shen, S., Hu, H., Chang, M., Chen, D., Wu, Y., Yuan, H., Wang, Y. 2023. Engineering banana-peel-derived biochar for the rapid adsorption of tetracycline based on double chemical activation. Resources, Conservation and Recycling, 190: 106821. Doi: 10.1016/j.resconrec.2022.106821

Zhu, S., Jiao, S., Liu, Z., Pang, G., Feng, S. 2014. High adsorption capacity for dye removal by CuZn hydroxyl double salts. Environmental science: nano, 1(2): 172-180. Doi: 10.1039/C3EN00078H